

Freezing of anisotropic spin clusters in $\text{La}_{1.98}\text{Sr}_{0.02}\text{CuO}_4$

M. Matsuda

The Institute of Physical and Chemical Research (RIKEN), Wako, Saitama 351-0198, Japan

Y. S. Lee, M. Greven,* M. A. Kastner, and R. J. Birgeneau
*Department of Physics and Center for Materials Science and Engineering,
Massachusetts Institute of Technology, Cambridge, Massachusetts 02139*

K. Yamada[†] and Y. Endoh
Department of Physics, Tohoku University, Sendai 980-0812, Japan

P. Böni
Laboratory for Neutron Scattering, PSI, CH-5232 Villigen PSI, Switzerland

S.-H. Lee
National Institute of Standards and Technology, NIST Center for Neutron Research, Gaithersburg, Maryland 20899

S. Wakimoto[‡] and G. Shirane
Department of Physics, Brookhaven National Laboratory, Upton, New York 11973
(Received 19 July 1999)

A spin-glass compound, $\text{La}_{1.98}\text{Sr}_{0.02}\text{CuO}_4$, shows quasi-three-dimensional magnetic ordering below ~ 40 K. A remarkable feature is that the magnetic correlation length along the orthorhombic a_{ortho} axis is much longer than that along the b_{ortho} axis, suggesting that the spin structure is closely related to the diagonal stripe structure. The spin-glass state can be expressed as a random freezing of quasi-three-dimensional spin clusters with anisotropic spin correlations ($\xi'_a \sim 160$ Å, $\xi'_b \sim 25$ Å, and $\xi'_c \sim 4.7$ Å at 1.6 K). The new magnetic state is important as an intermediate phase between the three-dimensional antiferromagnetic ordered phase in La_2CuO_4 and the incommensurate phase in $\text{La}_{1.95}\text{Sr}_{0.05}\text{CuO}_4$ in which the positions of the incommensurate peaks are rotated by 45° in reciprocal space about (π, π) from those observed in the superconducting La_2CuO_4 compounds.

74.72.Dn, 75.10.Jm, 75.50.Ee, 75.50.Lk

I. INTRODUCTION

Extensive studies on the high- T_c superconducting copper oxides have revealed an intimate connection between the magnetism and the superconductivity.¹ A detailed study of the spin dynamics in the superconducting $\text{La}_{2-x}\text{Sr}_x\text{CuO}_4$ system has been performed by Yamada *et al.*² The phase diagram of $\text{La}_{2-x}\text{Sr}_x\text{CuO}_4$ has been explored and it has been shown that the magnetic properties evolve dramatically with Sr doping. The parent material La_2CuO_4 shows three-dimensional (3D) long-range antiferromagnetic ordering below ~ 325 K.^{3,4} When Sr is doped in the material, the 3D antiferromagnetic ordering quickly disappears and, as originally predicted by Aharony *et al.*,⁵ the Néel state is replaced by a spin-glass phase. In this phase elastic magnetic Bragg rods, originating from two-dimensional (2D) spin correlations, develop gradually as shown by Sternlieb *et al.*⁶ and Keimer *et al.*⁷ In particular, Keimer *et al.* found that the magnetic peaks are almost elastic and relatively sharp in Q in $\text{La}_{1.96}\text{Sr}_{0.04}\text{CuO}_4$. Very recently, Wakimoto *et al.* studied the magnetic properties in the spin-glass phase ($0.03 \leq x \leq 0.05$) in detail elucidating the hole concentration dependence of the transition temperature and the spin correlations.⁸ Most importantly, they found incommensurate spin correlations in the spin-glass $\text{La}_{1.95}\text{Sr}_{0.05}\text{CuO}_4$ in which the positions of the incommensurate peaks were rotated by 45° in reciprocal space about (π, π) from those observed in Sr-richer superconducting compounds.

On the other hand, static magnetic ordering has also been observed in superconducting $\text{La}_{2-x}\text{Sr}_x\text{CuO}_4$. Suzuki *et al.*⁹ and Kimura *et al.*¹⁰ showed that sharp incommensurate magnetic Bragg peaks develop at low temperatures in superconducting $\text{La}_{1.88}\text{Sr}_{0.12}\text{CuO}_4$, in close analogy with the putative stripe ordering of holes and spins found in the $\text{La}_{2-y-x}\text{Nd}_y\text{Sr}_x\text{CuO}_4$ system.¹¹ Very recently, quasi-3D magnetic ordering has been observed in superconducting $\text{La}_2\text{CuO}_{4+\delta}$.¹² Thus, magnetic ordering takes place in the $\text{La}_{2-x}\text{Sr}_x\text{CuO}_4$ system with various levels of hole doping. It is essential to clarify the nature of the static magnetic behavior in order to understand the relationship between the spin-glass, the stripe, and the low temperature magnetic phase in the superconducting samples.

In this paper, we report on high-resolution elastic and inelastic neutron scattering studies in $\text{La}_{1.98}\text{Sr}_{0.02}\text{CuO}_4$. Previously, inelastic neutron scattering measurements with medium-resolution were performed on the same sample in order to study the magnetic excitations.¹³ The main purpose of the previous experiments was to compare the dynamic spin properties of the $x=0.02$ sample with those in $\text{La}_{1.96}\text{Sr}_{0.04}\text{CuO}_4$, in which the integrated susceptibility scales with E/T .⁷ Since the time that these experiments were performed, it has become evident that the static magnetic properties are also important as mentioned above. Stimulated by those findings, we aimed to clarify the static magnetic properties in the spin-glass phase of $\text{La}_{1.98}\text{Sr}_{0.02}\text{CuO}_4$, in which the 3D antiferromagnetic long-range ordering just disappears. The most interesting issue is how the long-range 3D antiferromagnetic ordering disappears and the spin-glass behavior appears with hole doping.

In this study we find that below ~ 40 K quasi-elastic magnetic peaks develop at the positions where magnetic Bragg peaks exist in La_2CuO_4 . This means that spin correlations develop perpendicular to the CuO_2 plane in addition to parallel to it, suggesting that the 2D spin fluctuations, which exist at high temperatures, at least in part freeze with freezing temperature enhanced due to the interplanar interaction. Our most important findings are that the spin correlations in the CuO_2 plane are anisotropic at low temperatures and that the spin directions in the spin clusters differs from that in pure La_2CuO_4 . The spin cluster dimension along the a_{ortho} axis (~ 160 Å) is ~ 6 times longer than that along the b_{ortho} axis (~ 25 Å) at 1.6 K. From these results, it is concluded that the spin-glass state can be described as a random freezing of quasi-3D spin clusters with anisotropic spin correlations.

The format of this paper is as follows: The scattering geometry used in this study is summarized in Sec. 2. Experimental details are described in Sec. 3. The experimental results of the elastic neutron measurements are presented and the spin structure of the short-range ordered state is summarized in Sec. 4. The experimental results on the inelastic neutron measurements are presented in Sec. 5. In Sec. 6 we discuss the magnetic properties of the spin-glass state.

II. SCATTERING GEOMETRY

Figure 1(a) shows the scattering geometry in the $(H, H, 0)$ scattering plane in the high-temperature tetragonal phase. $\text{La}_{1.98}\text{Sr}_{0.02}\text{CuO}_4$ undergoes a structural phase transition from tetragonal ($I4/mmm$) to orthorhombic ($Bmab$) structure at 485 K. Figure 1(b) shows the scattering geometry in the $(H, K, 0)$ scattering plane in the low-temperature orthorhombic phase. The structure is slightly distorted with the a_{ortho} and b_{ortho} axes almost along the diagonal directions of the a_{tetra} and b_{tetra} axes. Ideally, the experiments should be performed with a single domain crystal. However, four domains are expected to exist in real crystals since a twin structure is energetically stable. For small rectangular samples it is possible to prepare a single domain crystal by heating the sample above the transition temperature and then cooling it down while applying pressure along the a_{ortho} or b_{ortho} axis. However, the heat treatment is not efficient for large crystals so that preparation of a single domain sample is extremely difficult in practice. Consequently in this experiment, we were forced to use a four-domain crystal.

The scattering geometry for the four-domain crystal is shown in Fig. 1(c). $(H, K, L)_{\text{ortho}}$ and $(K, H, L)_{\text{ortho}}$ nuclear Bragg peaks are observed at nearby positions. As a result, four peaks are observed around $(1,1,0)_{\text{tetra}}$ and three peaks are observed around $(2,0,0)_{\text{tetra}}$ in the $(H, K, 0)$ scattering plane. Figure 2(a) shows an elastic scan (scan A as indicated in Fig. 1(c)) at $(2,0,0)_{\text{tetra}}$. The two side peaks at $(2,0,0)_{\text{tetra}}$ originate from two of the domains and the central peak, which is factor of ~ 2 larger than each side peak, originates from the other two domains. From these results, we estimate that the four domains are equally distributed. Due to the twin structure, the $(H, 0, L)_{\text{ortho}}$ and the $(0, K, L)_{\text{ortho}}$ scattering planes are superposed upon each other as shown in Fig. 1(d). Scan B in Fig. 1(d) corresponds to scan C in Fig. 1(c). Since the vertical resolution is quite broad, the $(2,0,0)_{\text{ortho}}$ ($(0,2,0)_{\text{ortho}}$) peak shown in Fig. 2(b) actually originates from two separate $(2,0,0)_{\text{ortho}}$ ($(0,2,0)_{\text{ortho}}$) peaks from two domains above and below the scattering plane.

There are two ways to express Miller indices; the high temperature tetragonal phase notation $(H, K, L)_{\text{tetra}}$ and the low temperature orthorhombic phase notation $(H, K, L)_{\text{ortho}}$. Since all of the results shown in this paper are observed in the orthorhombic phase and also obtained in the $(H, 0, L)_{\text{ortho}}$ and $(0, K, L)_{\text{ortho}}$ scattering planes, $(H, K, L)_{\text{ortho}}$ will be used to express Miller indices.

III. EXPERIMENTAL DETAILS

The single crystal of $\text{La}_{1.98}\text{Sr}_{0.02}\text{CuO}_4$ was grown from a non-stoichiometric CuO-rich solution.¹⁴ The dimensions of the plate-like shaped crystal are about $20 \times 20 \times 3$ mm³. The effective mosaic of the single crystal is less than 0.5° full-width-at-half-maximum. The Sr concentration was determined directly from an electron probe microanalysis

measurement and indirectly from neutron scattering measurements of the structural phase transition temperature, $T_{st}=485$ K. The lattice constants are $a_{ortho}=5.333$ Å, $b_{ortho}=5.414$ Å, and $c=13.098$ Å ($b/a=1.015$) at 1.6 K. The $\text{La}_{1.98}\text{Sr}_{0.02}\text{CuO}_4$ crystal is the same one as used in Ref. 13. We observe that weak but sharp magnetic Bragg peaks gradually develop below ~ 165 K at the positions where magnetic Bragg peaks exist in La_2CuO_4 . However, the volume fraction is estimated to be less than 10% if $0.3\mu_B$ is assumed for the Cu moment as in an oxygen-rich La_2CuO_4 ($T_N=185$ K). We assume that the 3D magnetic peaks come from a small fraction of the volume where the Sr and/or oxygen concentration is below the critical value. Since the magnetic signals which are discussed in this paper originate from diffuse scattering, the sharp peaks from the 3D Néel phase can easily be separated from the 2D spin glass signals by avoiding the regions around $(1, 0, \textit{even})_{ortho}$ and $(0, 1, \textit{odd})_{ortho}$.

The neutron scattering experiments were carried out on the three-axis spectrometers H7 and H8 at the Brookhaven High-Flux Beam Reactor, on the three-axis spectrometer TASP at the cold neutron guide at the PSI-SINQ Facility, and on the three-axis spectrometer SPINS at the cold neutron guide at the NIST Center for Neutron Research. For most of the elastic measurements, the horizontal collimator sequences were $40'-40'-S-40'-80'$ and $32'-40'-S-40'-220'$ with a fixed incident neutron energy of $E_i=5$ meV. For the inelastic measurements, the horizontal collimator sequences were $20'-20'-S-20'-80'$ with $E_i=14.7$ meV and $72'-80'-S-80'-80'$ with $E_f=8$ meV for lower energies ($E \leq 4$ meV) and $40'-40'-S-40'-80'$ with $E_f=14.7$ meV for $E=10$ meV. Pyrolytic graphite (002) was used as both monochromator and analyzer. Contamination from higher-order neutrons was effectively eliminated using Be filters for $E_i=5$ meV and pyrolytic graphite filters for $E_i=14.7$ meV and $E_f=14.7$ meV. No filter was used for measurements with $E_f=8$ meV at TASP since the population of the higher-order beam is considerably reduced. The single crystal was oriented in the $(H, 0, L)_{ortho}$ and $(0, K, L)_{ortho}$ scattering planes. For the elastic measurements the sample was mounted in a helium pumped cryostat while for the inelastic measurements the sample was mounted in a closed cycle refrigerator.

IV. STATIC MAGNETIC PROPERTIES

A. Neutron Elastic Experiments

Figure 3(a) shows an elastic neutron scan at $(H, 0, -0.3)$ at 1.6 K. A sharp peak is observed at $H=1$. If the magnetic correlations were isotropic in the ab plane and the correlations were purely two dimensional, it would be expected that two sharp equi-intense peaks would be observed at $H=0.985$ ($K=1$) and 1.¹⁵ The data in Fig. 3(a) indicate that there are spin correlations along the c axis and/or that spin correlations are anisotropic. The temperature dependence of the intensity at $(1, 0, -0.3)$ is shown in Fig. 3(b). The filled circles represent data measured with $E_i=5$ meV ($\Delta E=0.25$ meV); the intensity gradually develops below ~ 40 K. The open circles represent the data measured with $E_i=14.7$ meV ($\Delta E=0.9$ meV); the intensity starts to increase at ~ 80 K and the development of the intensity is much broader. These results are consistent with those observed by Keimer *et al.* in $\text{La}_{1.96}\text{Sr}_{0.04}\text{CuO}_4$.⁷ Specifically, this means that the magnetic signal is quasi-elastic rather than truly elastic so that the temperature dependence of the intensity depends on the energy window.

B. Spin Structure

Figures 4(a) and 4(b) show the L dependence of the magnetic elastic peaks at $(1, 0, L)$ and $(0, 1, L)$ at 1.6 K, respectively. The background estimated from the high temperature data (60 K) was subtracted so that the remaining signal is purely magnetic. Broad peaks are observed at $(1, 0, \textit{even})$ where magnetic Bragg peaks exist in La_2CuO_4 . There are some characteristic features. Firstly the peaks are broad, indicating that the spin correlations along the c axis are short-ranged. Secondly, the magnetic intensity at $(1, 0, \textit{even})$ initially increases with increasing L , in contrast to the behavior found for the magnetic Bragg intensities in pure La_2CuO_4 . Lastly, the magnetic intensities at $(1, 0, L)$ are much larger than those at $(0, 1, L)$. From these results, one can deduce that spin clusters are formed in $\text{La}_{1.98}\text{Sr}_{0.02}\text{CuO}_4$. However, the spin clusters have a different geometrical structure from that in pure La_2CuO_4 .

The magnetic Bragg intensity is proportional to

$$\left[\mathbf{S}_\perp f(Q) \sum_j \exp(i\mathbf{Q} \cdot \mathbf{R}_j) \right]^2 \quad (1)$$

where \mathbf{S}_\perp , $f(Q)$, and \mathbf{R}_j are the copper spin component perpendicular to \mathbf{Q} , the magnetic form factor, and the copper ion positions, respectively. In pure La_2CuO_4 , the magnetic intensities at $(1, 0, \textit{even})$ are just proportional to $f(Q)^2$,

which is approximately constant for the range of L 's considered here¹⁶, since the copper spins point along the b axis perpendicular to the (HOL) scattering plane and $\sum \exp(i\mathbf{Q} \cdot \mathbf{R}_j)$ at $(1,0, \text{even})$ is calculated to be constant from the 3D spin structure with the antiferromagnetic propagation vector $\hat{\tau} \parallel \hat{\mathbf{a}}_{\text{ortho}}$.

The simplest model to explain the increase of the intensity with increasing L along both $(1,0,L)$ and $(0,1,L)$ is that the cluster antiferromagnetic spin is randomly directed within the ab plane. In this case, the intensity would vary like

$$[\mathbf{S}_{\perp} f(Q)]^2 = \frac{1}{2} [1 + \sin^2 \theta(L)] S^2 f(Q)^2 \quad (2)$$

where $\theta(L)$ is the angle that the Q -vector of the $(1,0,L)$ or $(0,1,L)$ reflection makes with the ab plane. We will justify this model after first discussing the spatial geometry of the frozen clusters. We should note that a result equivalent to Eq. (2) is obtained by fixing the spin direction along $(H, H, 0)$ or by assuming equal admixtures of 3D correlated phases where the spin vector \mathbf{S} is along or perpendicular to $\hat{\tau} (\parallel \hat{\mathbf{a}}_{\text{ortho}})$.

C. Anisotropic Spin Correlations

Figures 5(a) and 5(b) show elastic neutron scans at $(H, 0, 2.2)$ and $(H, 0, 3.2)$ at 1.6 K, respectively. The background estimated at $T=60$ K was subtracted so the remaining scattering is entirely magnetic. A sharp and intense peak is observed at $(1,0,2.2)$, whereas, a broad peak is observed at $(0,1,3.2)$ and a sharp peak with reduced integrated intensity is observed at $(1,0,3.2)$. These results strongly indicate that the spin correlations are anisotropic in the ab plane, that is, the spin correlations are longer along the a_{ortho} axis than along the b_{ortho} axis. If the magnetic correlations were isotropic in the ab plane, it would be expected that two sharp peaks would be observed at $H=0.985$ ($K=1$) and 1. The fact that the measured intensities at $(1,0, \text{even})$ are larger than those at $(0,1, \text{odd})$ is a resolution effect arising from both the broadening along b_{ortho} and the fact that the coarse vertical resolution effectively integrates the peaks at $(1,0, \text{even})$ which are elongated perpendicular to the scattering plane as shown in the inset of Fig. 4(b).

The solid lines in Figs. 4(a), 4(b), 5(a), and 5(b) are the calculated profiles using as the intrinsic line shape 3D squared Lorentzians convoluted with the instrumental resolution function:

$$L(H, K, L, E) = \sum_{\text{even}, \text{odd}} \left[\left(\frac{1}{\xi_a'^2 (H-1)^2 + \xi_b'^2 K^2 + \xi_c'^2 (L - \text{even})^2 + 1} \right)^2 + \left(\frac{1}{\xi_a'^2 H^2 + \xi_b'^2 (K-1)^2 + \xi_c'^2 (L - \text{odd})^2 + 1} \right)^2 \right] \times \frac{1}{E^2 + \Gamma^2} \quad (3)$$

where ξ_a' , ξ_b' , ξ_c' , and Γ represent the elastic spin correlation lengths or cluster sizes along the a_{ortho} axis, b_{ortho} axis, and c axis and the energy width, respectively. In order to describe spin correlations which have finite lengths three-dimensionally, one might instead have used 3D Lorentzians:

$$L(H, K, L, E) = \sum_{\text{even}, \text{odd}} \left(\frac{1}{\xi_a'^2 (H-1)^2 + \xi_b'^2 K^2 + \xi_c'^2 (L - \text{even})^2 + 1} + \frac{1}{\xi_a'^2 H^2 + \xi_b'^2 (K-1)^2 + \xi_c'^2 (L - \text{odd})^2 + 1} \right) \times \frac{1}{E^2 + \Gamma^2}. \quad (4)$$

However, this function has long tails in Q space and does not decay as rapidly as the observed data do. Equation (3) describes the observed data well so that ξ_a' , ξ_b' , and ξ_c' can be estimated quite reliably. We note that the Lorentzian squared form is the expected profile for frozen 3D random clusters with sharp boundaries.

In the calculation the spin structure models described in Sec. 4-B, all of which give the same L -dependence of the intensity, are assumed. The parameters used are $\xi_a'=160$ Å, $\xi_b'=25$ Å, and $\xi_c'=4.7$ Å. Γ is fixed at 0.01 meV which is determined experimentally. The calculation describes the observed data at $(1,0,L)$, $(0,1,L)$, $(H,0,2.2)$, and $(H,0,3.2)$ reasonably well. The small peaks at $(1,0, \text{odd})$ and $(0,1, \text{even})$ in Figs. 4(a) and 4(b) originate from the tails of the broad $(0,1, \text{odd})$ and $(1,0, \text{even})$ peaks, respectively. Surprisingly, it is found that ξ_a' is about 6 times longer than ξ_b' . The average distance between doped holes in the CuO_2 plane is ~ 30 Å in $\text{La}_{1.98}\text{Sr}_{0.02}\text{CuO}_4$, which is similar to ξ_b' but much smaller than ξ_a' . $\xi_c'=4.7$ Å indicates that the cluster size perpendicular to the CuO_2 plane is similar to the

distance between nearest-neighbor CuO_2 planes. A schematic figure of the spin configuration in the ab plane at 1.6 K is shown in Fig. 6. As mentioned in Sec. 4-B the spin easy axis cannot be determined uniquely from this study, but the data are consistent with a model in which the cluster antiferromagnetic spin direction is random in the ab plane.

V. MAGNETIC EXCITATIONS

Figure 7 shows neutron inelastic scans at the energies 2, 4, and 10 meV measured at 35 K. The spectra at 2 and 4 meV show a peak at $H=1$ and a broad tail at the left side ($H < 1$). On the other hand, the spectrum at 10 meV shows a broad and symmetric peak centered at $H \sim 0.99$. From the results shown in Sec. 4-C, the peak profiles at 2 and 4 meV appear to reflect the static anisotropic spin correlations. Therefore, the spectra can be described with one sharp peak at $H=1$ and one broad peak at $H=0.985$ ($K=1$). The symmetric peak profile at 10 meV, however, indicates that the dynamical spin correlations become isotropic at high energies.

Figure 8 shows the temperature dependence of the inelastic neutron spectra at 1.5 meV. The spectrum at 35 K is consistent with that observed at 2 meV and 35 K. The spectrum becomes more symmetric with increasing temperature. These results indicate that the dynamic spin correlations in the ab plane are anisotropic at both low energies and low temperatures and become more isotropic at both high energies and high temperatures.

VI. DISCUSSION

The spin correlations in the spin-glass phase of $\text{La}_{1.98}\text{Sr}_{0.02}\text{CuO}_4$ have been clarified in this study. The static spin correlations are not simply finite-size versions of the Néel state spin structure in pure La_2CuO_4 . The characteristic features are as follows: (i) The spin cluster dimensions in the ab plane are highly anisotropic at low temperatures. (ii) The anisotropic behavior has both temperature and energy dependences. (iii) The cluster antiferromagnetic spin direction appears to be randomly oriented within the ab plane.

The anisotropic spin correlations in the ab plane are suggestive of the stripe phase found in $\text{La}_{2-y-x}\text{Nd}_y\text{Sr}_x\text{CuO}_4$.¹¹ However, the spin correlations in $\text{La}_{1.98}\text{Sr}_{0.02}\text{CuO}_4$ are different from those in $\text{La}_{2-y-x}\text{Nd}_y\text{Sr}_x\text{CuO}_4$. In $\text{La}_{2-y-x}\text{Nd}_y\text{Sr}_x\text{CuO}_4$ the hole/spin stripes run along the b_{tetra} (a_{tetra}) axis so that the magnetic domains should be elongated along the a_{tetra} (b_{tetra}) axis. These axes are rotated by 45° in the ab plane from the a_{ortho} axis along which spin correlations are longer in $\text{La}_{1.98}\text{Sr}_{0.02}\text{CuO}_4$. Interestingly, the spin correlations in $\text{La}_{1.98}\text{Sr}_{0.02}\text{CuO}_4$ have the same geometry as those predicted theoretically for the low concentration hole-doped system. A Hubbard model calculation on a two-dimensional square lattice has been performed by Schulz¹⁷ and by Kato *et al.*¹⁸ They find that a diagonally modulated spin density wave state (diagonal stripe state) is stable when the electron density is close to half-filling. In the diagonal state, the hole/spin stripes run along the a_{ortho} or b_{ortho} axis, which is rotated by 45° in the ab plane from the a_{tetra} (b_{tetra}) axis along which the stripes run in $\text{La}_{2-y-x}\text{Nd}_y\text{Sr}_x\text{CuO}_4$. Since the spin ordering observed in $\text{La}_{1.98}\text{Sr}_{0.02}\text{CuO}_4$ is short-ranged, the long-range diagonal stripe structure is not realized in this compound. However, short-range spin ordering with anisotropic spin correlations elongated along the a_{ortho} axis can be considered as a precursor phenomenon for the diagonal stripe ordering. It also seems apparent that the anisotropic spin correlations in $\text{La}_{1.98}\text{Sr}_{0.02}\text{CuO}_4$ are directly related to the incommensurate spin correlations observed in $\text{La}_{1.95}\text{Sr}_{0.05}\text{CuO}_4$, in which the incommensurate peaks are rotated by 45° in reciprocal space about (π, π) from those observed in Sr-rich superconducting compounds with $x \geq 0.06$.⁸ The diagonal stripe state is evidently more stable in this compound.

The connection with the results in $\text{La}_{1.95}\text{Sr}_{0.05}\text{CuO}_4$ can be made quantitative. In the diagonal stripe phase, Wakimoto *et al.* observe peaks displaced along b_{ortho} by a distance $\pm\delta$ where $\delta \simeq 2\pi x/b_{\text{tetra}}$ with x the Sr^{2+} concentration. Very recently, Matsuda *et al.* have found that $\delta \simeq 2\pi x/b_{\text{ortho}}$ in the highly insulating spin-glass sample $\text{La}_{1.976}\text{Sr}_{0.024}\text{CuO}_4$.¹⁹ Therefore, for $x=0.02$, $\delta \simeq 0.023 \text{ \AA}^{-1}$. We tried to fit the observed data in Figs. 4 and 5 with the diagonal stripe model with δ fixed at 0.023 \AA^{-1} . The data can be reasonably fitted with $\xi'_a = 160 \text{ \AA}$, $\xi'_b = 50 \text{ \AA}$, and $\xi'_c = 4.7 \text{ \AA}$. It is noted that ξ'_b is still short and the spin correlations are slightly anisotropic in the CuO_2 plane. Thus the measured line shape in $\text{La}_{1.98}\text{Sr}_{0.02}\text{CuO}_4$ is consistent with the diffraction profile expected from an array of disordered stripes locally oriented along a_{ortho} .

As mentioned in Sec. 4-B the L -dependence of the magnetic intensities is well described by a model in which the AF spin of a given cluster is randomly oriented in the ab plane. The equivalent result is obtained for the cluster staggered spin along a_{tetra} or b_{tetra} or randomly along both a_{ortho} and b_{ortho} . In the Néel state of pure La_2CuO_4 the spin is along b_{ortho} while just above $T_N=325 \text{ K}$, that is, at 328 K when the correlation length is about 800 \AA (Ref. 4) the spin is randomly oriented in the ab plane. Because of the latter result it seems physically plausible that in the frozen spin clusters below 40 K in $\text{La}_{1.98}\text{Sr}_{0.02}\text{CuO}_4$ of dimensions $160 \text{ \AA} \times 25 \text{ \AA}$ the spin direction would also be random. This is consistent with the fact that the net Ising anisotropy favoring the b_{ortho} axis from the Dzyaloshinsky-Moriya

interaction is only about 0.1 K in energy. We should note that in all cases we assume that the propagation vector of the AF order is along a_{ortho} in order to account for the pronounced peaks at $(1, 0, L)$ for L *even* alone.

One interesting and important question is why anisotropic but short-range correlations are achieved at low temperatures in our sample of $\text{La}_{1.98}\text{Sr}_{0.02}\text{CuO}_4$ whereas long-range diagonal incommensurate order occurs in $\text{La}_{1.95}\text{Sr}_{0.05}\text{CuO}_4$. Here, we speculate that the primary difference is not the hole concentration but rather the method of crystal growth. The $x=0.05$ crystal studied by Wakimoto *et al.* was grown with the traveling-solvent-floating-zone technique which is crucible-free whereas the $x=0.02$ crystal studied here was grown in a platinum crucible. It is known that in the latter case some platinum is incorporated into the crystal, that is, Pt^{2+} replaces Cu^{2+} . In that case, the Pt^{2+} impurities would exert an effective random field on the incipient hole stripes there by destroying the long-range order and causing the system to break up into finite size clusters²⁰ as we indeed observe experimentally. We need further studies using a Pt-free crystal with a low hole concentration in order to check whether the short-range correlations originate from Pt impurities or not.

We now discuss the results of the inelastic measurements. In the previous study on $\text{La}_{1.98}\text{Sr}_{0.02}\text{CuO}_4$,¹³ the scaling behavior with E/T of the integrated dynamical spin susceptibility was observed in the energy range $3 \leq E \leq 9$ meV. A clear deviation from the scaling function was observed at low temperatures in the energy range $E \leq 2$ meV. Similar behavior was also observed in the crucible-grown $\text{La}_{1.96}\text{Sr}_{0.04}\text{CuO}_4$ crystal studied by Keimer *et al.*⁷ In Ref. 13 it was argued that the susceptibility is suppressed at low energies due to the out-of-plane anisotropy. From our new results, it also appears to be possible that the observed susceptibility is suppressed at low energies and low temperatures because the broad peak at $(0, 1, L)$, which originates from the short correlation length along the b_{ortho} axis, was not properly integrated in the experiments of Ref. 13. Further studies are needed in order to determine the important features determining the dynamical spin susceptibility at low energies and low temperatures.

ACKNOWLEDGMENTS

We would like to thank Y. Hidaka for providing us with the single crystal of $\text{La}_{1.98}\text{Sr}_{0.02}\text{CuO}_4$. We would also like to thank V. J. Emery, K. Hirota, K. Machida, and J. Tranquada for stimulating discussions. This study was supported in part by the U.S.-Japan Cooperative Program on Neutron Scattering operated by the United States Department of Energy and the Japanese Ministry of Education, Science, Sports and Culture and by a Grant-in-Aid for Scientific Research from the Japanese Ministry of Education, Science, Sports and Culture. Work at Brookhaven National Laboratory was carried out under Contract No. DE-AC02-98CH10886, Division of Material Science, U.S. Department of Energy. The research at MIT was supported by the National Science Foundation under Grant No. DMR97-04532 and by the MRSEC Program of the National Science Foundation under Award No. DMR98-08941.

* Present address: Department of Applied Physics, Stanford University, Stanford, California 94305

† Present address: Institute for Chemical Research, Kyoto University, Gokasho, Uji 610-0011, Japan

‡ Also at Department of Physics, Massachusetts Institute of Technology, Cambridge, Massachusetts 02139

¹ M. A. Kastner, R. J. Birgeneau, G. Shirane, and Y. Endoh, *Rev. Mod. Phys.* **70**, 897 (1998).

² K. Yamada, C. H. Lee, K. Kurahashi, J. Wada, S. Wakimoto, S. Ueki, H. Kimura, Y. Endoh, S. Hosoya, G. Shirane, R. J. Birgeneau, M. Greven, M. A. Kastner, and Y. J. Kim, *Phys. Rev. B* **57**, 6165 (1998).

³ D. Vaknin, S. K. Shih, D. E. Moncton, D. C. Johnston, J. Newsam, C. R. Safinya, and H. King, *Phys. Rev. Lett.* **58**, 2802 (1987).

⁴ R. J. Birgeneau, M. Greven, M. A. Kastner, Y. S. Lee, B. O. Wells, Y. Endoh, K. Yamada, and G. Shirane, *Phys. Rev. B* **59**, 13788 (1999).

⁵ A. Aharony, R. J. Birgeneau, A. Coniglio, M. A. Kastner, and H. E. Stanley, *Phys. Rev. Lett.* **60**, 1330 (1988).

⁶ B. J. Sternlieb, G. M. Luke, Y. J. Uemura, T. M. Riseman, J. H. Brewer, P. M. Gehring, K. Yamada, Y. Hidaka, T. Murakami, T. R. Thurston, and R. J. Birgeneau, *Phys. Rev. B* **41**, 8866 (1990).

⁷ B. Keimer, N. Belk, R. J. Birgeneau, A. Cassanho, C. Y. Chen, M. Greven, M. A. Kastner, A. Aharony, Y. Endoh, R. W. Erwin, and G. Shirane, *Phys. Rev. B* **46**, 14034 (1992).

⁸ S. Wakimoto, R. J. Birgeneau, Y. Endoh, P. M. Gehring, K. Hirota, M. A. Kastner, S. H. Lee, Y. S. Lee, G. Shirane, S. Ueki, and K. Yamada, *Phys. Rev. B* **60**, R769 (1999).

⁹ T. Suzuki, T. Goto, K. Chiba, T. Shinoda, T. Fukase, H. Kimura, K. Yamada, M. Ohashi, and Y. Yamaguchi, *Phys. Rev. B* **57**, 3229 (1998).

- ¹⁰ H. Kimura, K. Hirota, H. Matsushita, K. Yamada, Y. Endoh, S.-H. Lee, C. F. Majkrzak, R. Erwin, G. Shirane, M. Greven, Y. S. Lee, M. A. Kastner, and R. J. Birgeneau, Phys. Rev. B **59**, 6517 (1999).
- ¹¹ J. M. Tranquada, J. D. Axe, N. Ichikawa, Y. Nakamura, S. Uchida, and B. Nachumi, Phys. Rev. B **54**, 7489 (1996).
- ¹² Y. S. Lee, R. J. Birgeneau, M. A. Kastner, Y. Endoh, S. Wakimoto, K. Yamada, R. W. Erwin, S.-H. Lee, and G. Shirane, Phys. Rev. B **60**, 3643 (1999).
- ¹³ M. Matsuda, R. J. Birgeneau, Y. Endoh, Y. Hidaka, M. A. Kastner, K. Nakajima, G. Shirane, T. R. Thurston, K. Yamada, J. Phys. Soc. Jpn. **62**, 1702 (1993).
- ¹⁴ Y. Hidaka, Y. Enomoto, M. Suzuki, M. Oda, and T. Murakami, J. Crystal Growth **85**, 581 (1987).
- ¹⁵ See for example, the analogous data in pure La_2CuO_4 above T_N in Fig. 2 of Ref. 4.
- ¹⁶ T. Freltoft, G. Shirane, S. Mitsuda, J. P. Remeika, and A. S. Cooper, Phys. Rev. B **37**, 137 (1988).
- ¹⁷ H. J. Schulz, J. Phys. France. **50**, 2833 (1989).
- ¹⁸ M. Kato, K. Machida, H. Nakanishi, and M. Fujita, J. Phys. Soc. Jpn. **59**, 1047 (1990).
- ¹⁹ M. Matsuda, R. J. Birgeneau, Y. Endoh, M. Fujita, M. A. Kastner, G. Shirane, S. Wakimoto, and K. Yamada, unpublished.
- ²⁰ R. J. Birgeneau, J. Magn. Magn. Mat. **177**, 1 (1998).

FIG. 1. Diagrams of the reciprocal lattice in the $(H, K, 0)$ scattering zone in the tetragonal phase (a) and the orthorhombic phase (b) for a single domain crystal. The lower figures show diagrams of the reciprocal lattice in the $(H, K, 0)$ scattering zone (c) and in the $(H, 0, L)_{ortho}$ scattering zone (d) for a crystal with four domains.

FIG. 2. The results of elastic neutron scans A and B as shown in Figs. 1(c) and (d), respectively.

FIG. 3. (a) An elastic scan at $(1, 0, -0.3)$ at 1.6 K. The solid line is a guide to the eye. The broken lines show the centers of the peaks $(1, 0, -0.3)$ and $(0, 1, -0.3)$ determined from the nuclear Bragg peaks $(2, 0, 0)$ and $(0, 2, 0)$. (b) Temperature dependence of the peak intensity at $(1, 0, -0.3)$ measured with the two different incident neutron energies 5 meV ($\Delta E=0.25$ meV) and 14.7 meV ($\Delta E=0.9$ meV). The two sets of the data are normalized at 1.6 K.

FIG. 4. Elastic scans along $(1, 0, L)$ (a) and along $(0, 1, L)$ (b) at 1.6 K. The background intensities measured at 60 K are subtracted. The solid lines shows the results of calculations with $\xi'_a=160$ Å, $\xi'_b=25$ Å, and $\xi'_c=4.7$ Å. The inset shows the schematic configuration of the broad magnetic peaks. The arrows a and b show scan trajectories in (a) and (b), respectively.

FIG. 5. Elastic scans along $(H, 0, 2.2)$ (a) and along $(H, 0, 3.2)$ (b) at 1.6 K. The background intensities measured at 60 K are subtracted. The broken lines show the centers of the peaks $(1, 0, L)$ and $(0, 1, L)$ ($L=2.2$ and 3.2) determined from the nuclear Bragg peak positions. The solid lines show the results of calculations with $\xi'_a=160$ Å, $\xi'_b=25$ Å, and $\xi'_c=4.7$ Å. The inset shows the schematic configuration of the broad magnetic peaks. The arrows show scan trajectories.

FIG. 6. A possible spin structure model in the spin-glass phase of $\text{La}_{1.98}\text{Sr}_{0.02}\text{CuO}_4$. (a) Spin easy axes are random between spin clusters. The arrows show the spin easy axis of a sublattice of each antiferromagnetic cluster. (b) In-plane spin arrangement of the spin cluster at $T=1.6$ K with a spin easy axis along the b_{ortho} axis.

FIG. 7. Inelastic scans along $(H, 0, -0.6)$ at 35 K as a function of energy. The solid lines are guides to the eye. The broken lines show the centers of the peaks $(1, 0, -0.6)$ and $(0, 1, -0.6)$ determined from the nuclear Bragg peak positions. The inset shows the schematic configuration of the broad magnetic peaks. The arrow shows a scan trajectory.

FIG. 8. Inelastic scans along $(H, 0, 0.6)$ at 1.5 meV as a function of temperature. The solid lines are guides to the eye. The broken lines show the centers of the peaks $(1, 0, 0.6)$ and $(0, 1, 0.6)$ determined from the nuclear Bragg peak positions.

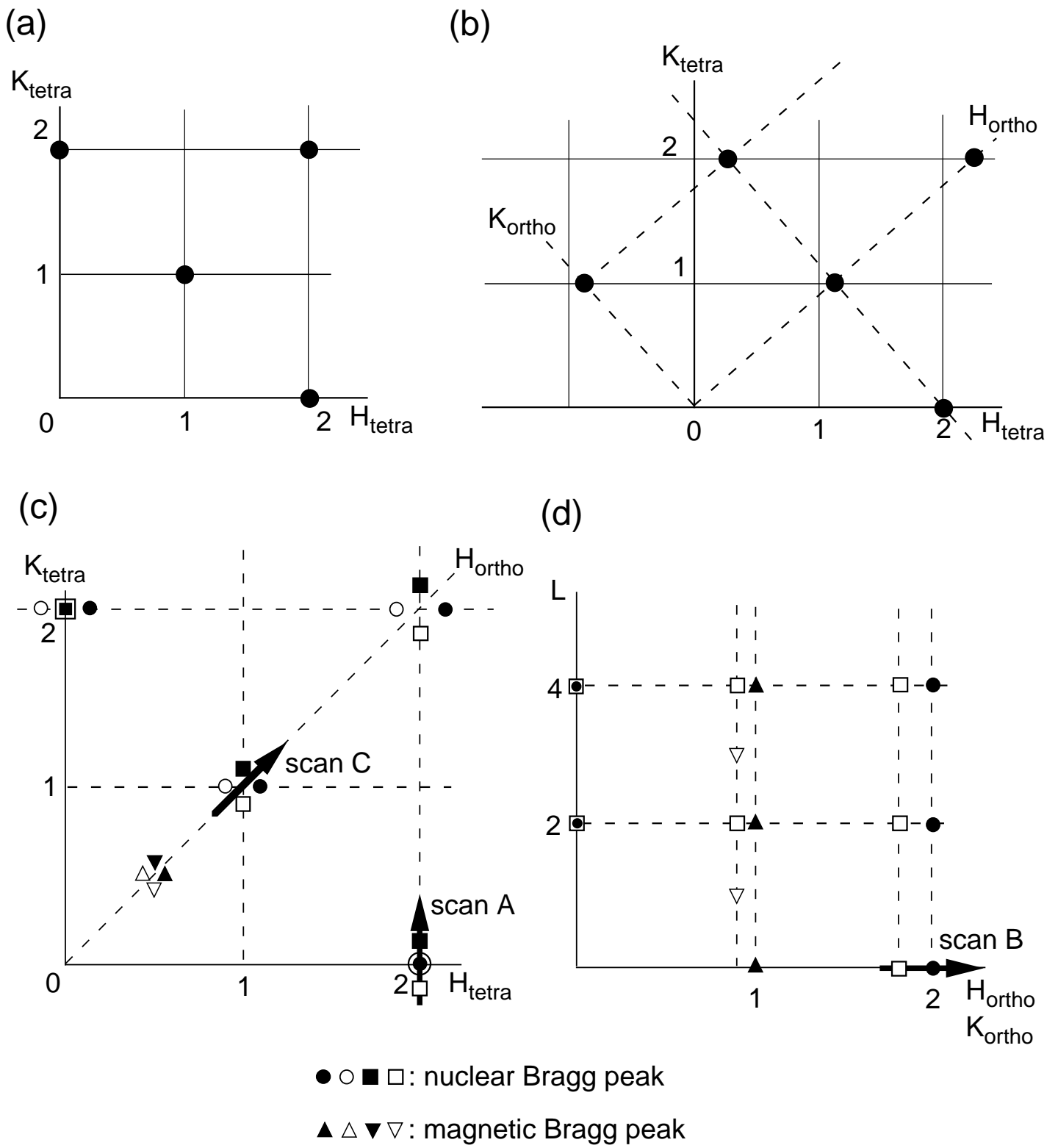
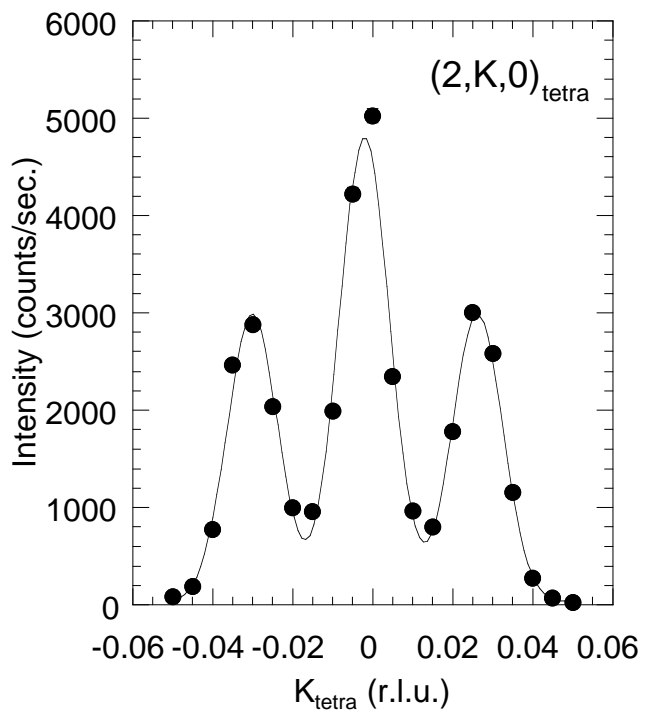


Fig. 1 Matsuda *et al.*

(a) scan A



(b) scan B

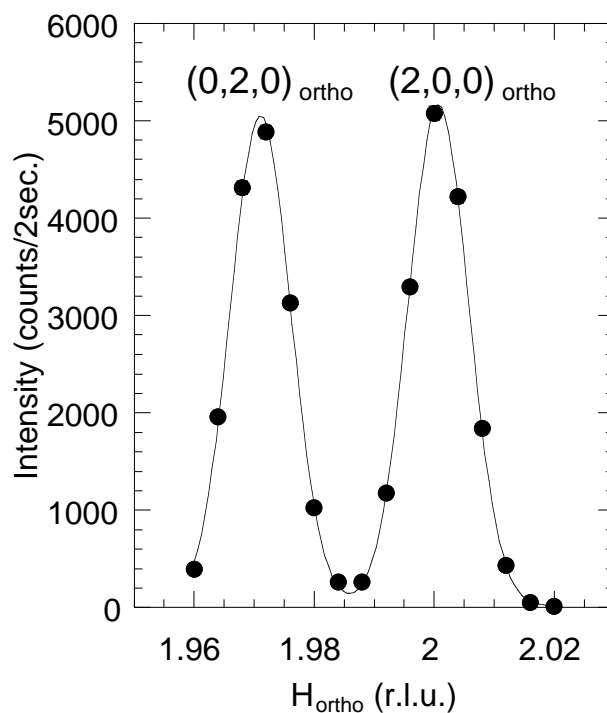


Fig. 2 Matsuda *et al.*

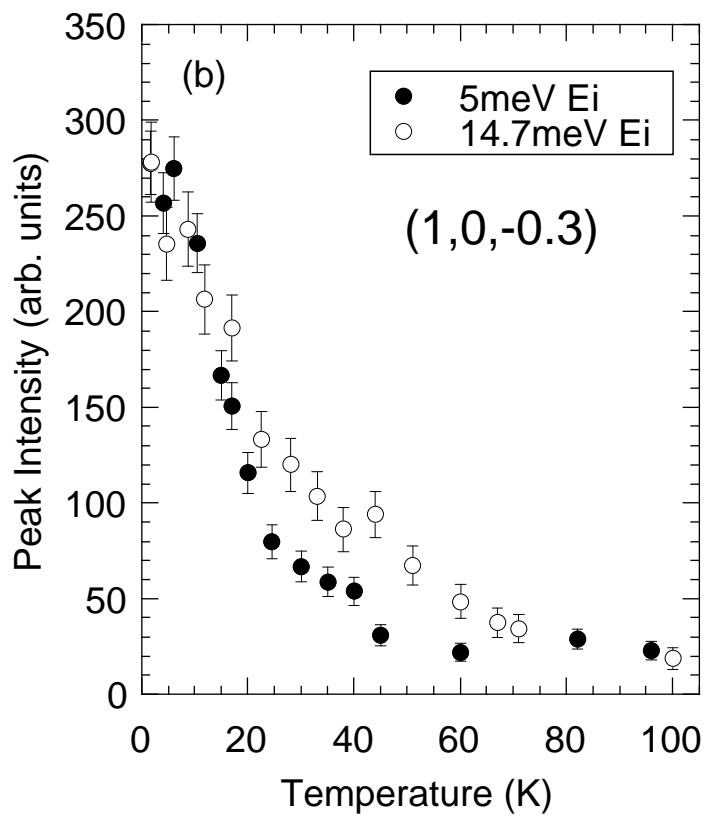
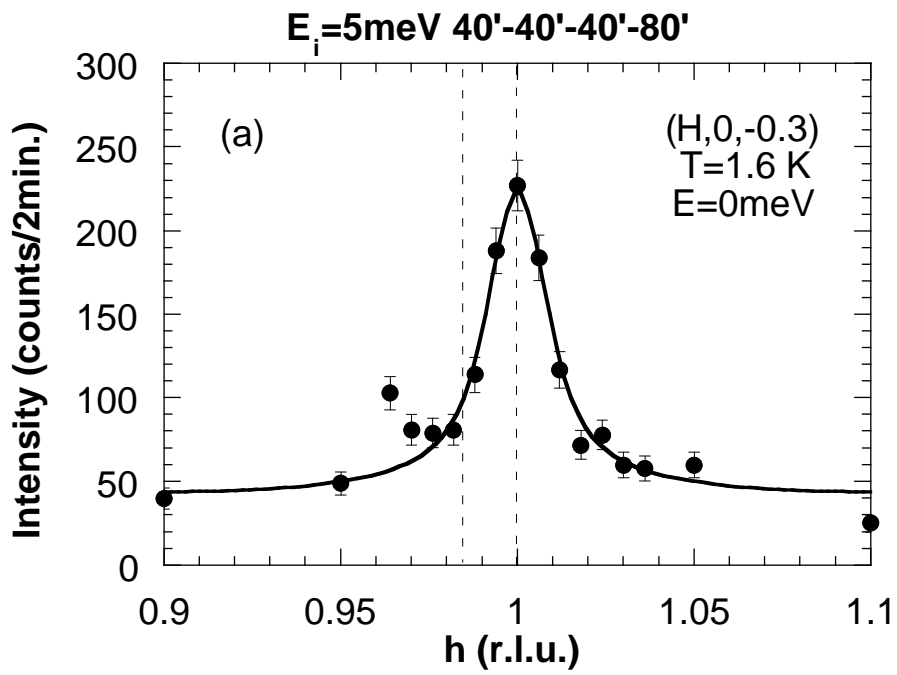


Fig. 3 Matsuda *et al.*

$E_i=5\text{meV}$, $32^\circ\text{-}40^\circ\text{-}40^\circ\text{-}220^\circ$, $T=1.5\text{ K}$

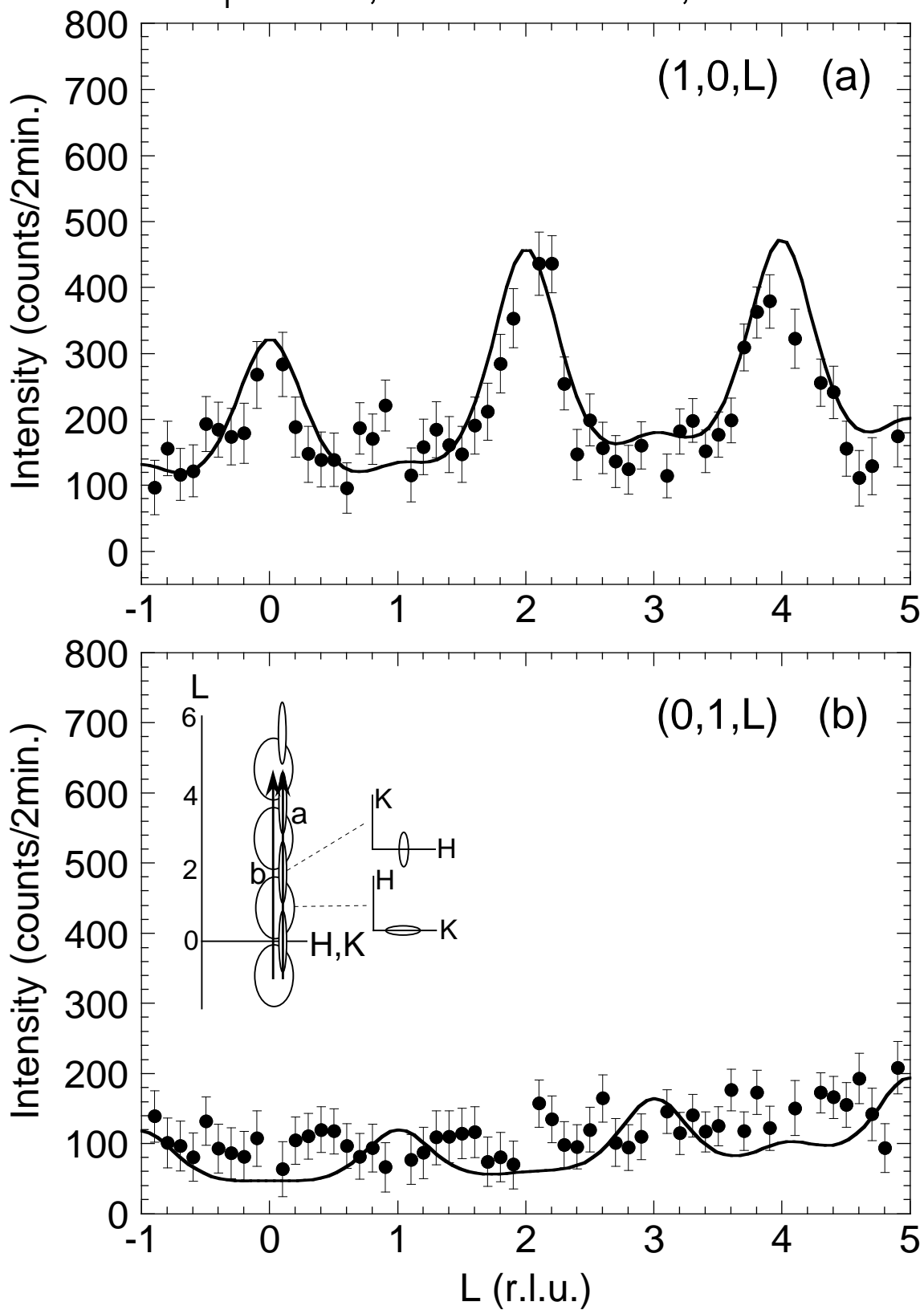


Fig. 4 Matsuda *et al.*

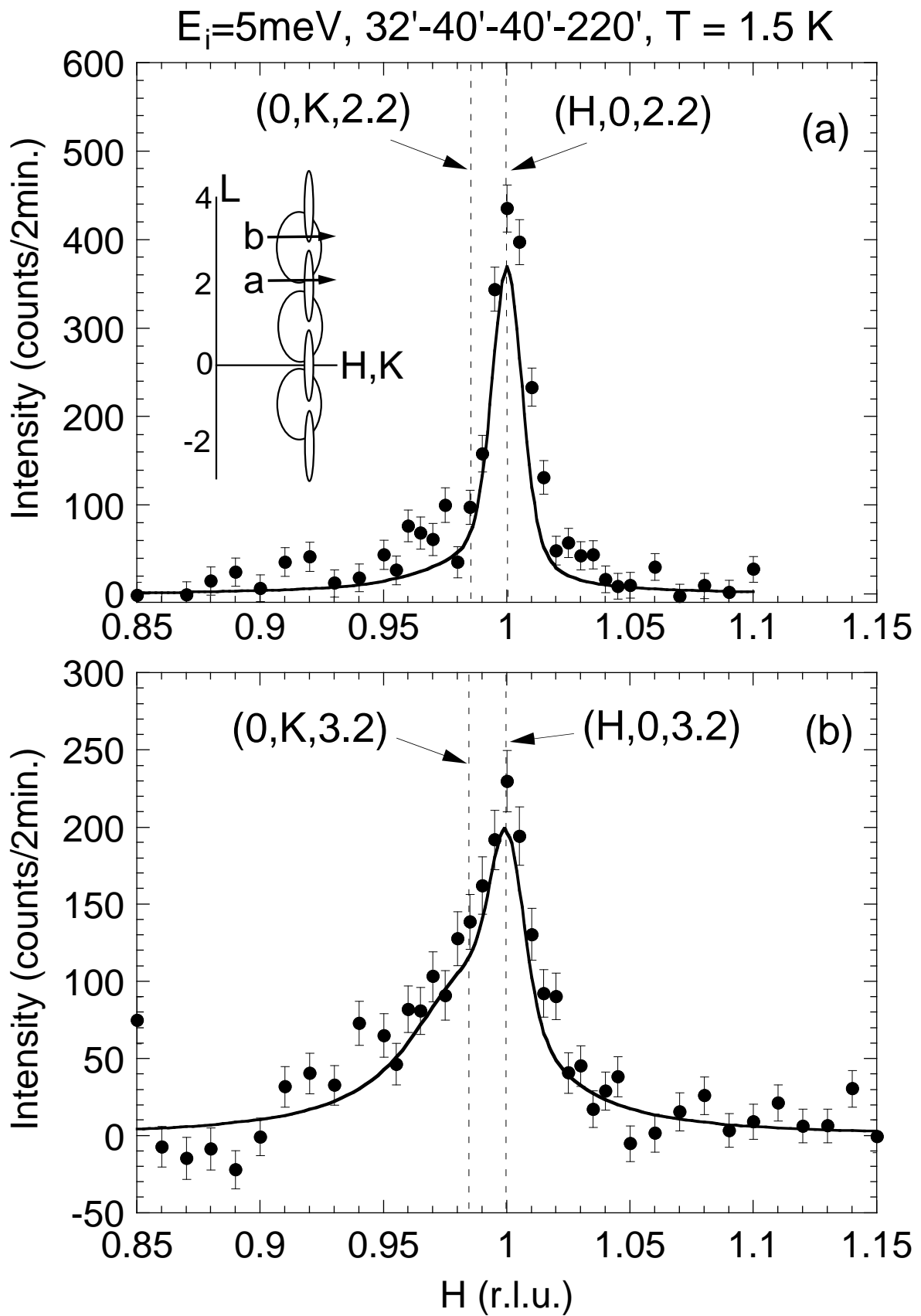


Fig. 5 Matsuda *et al.*

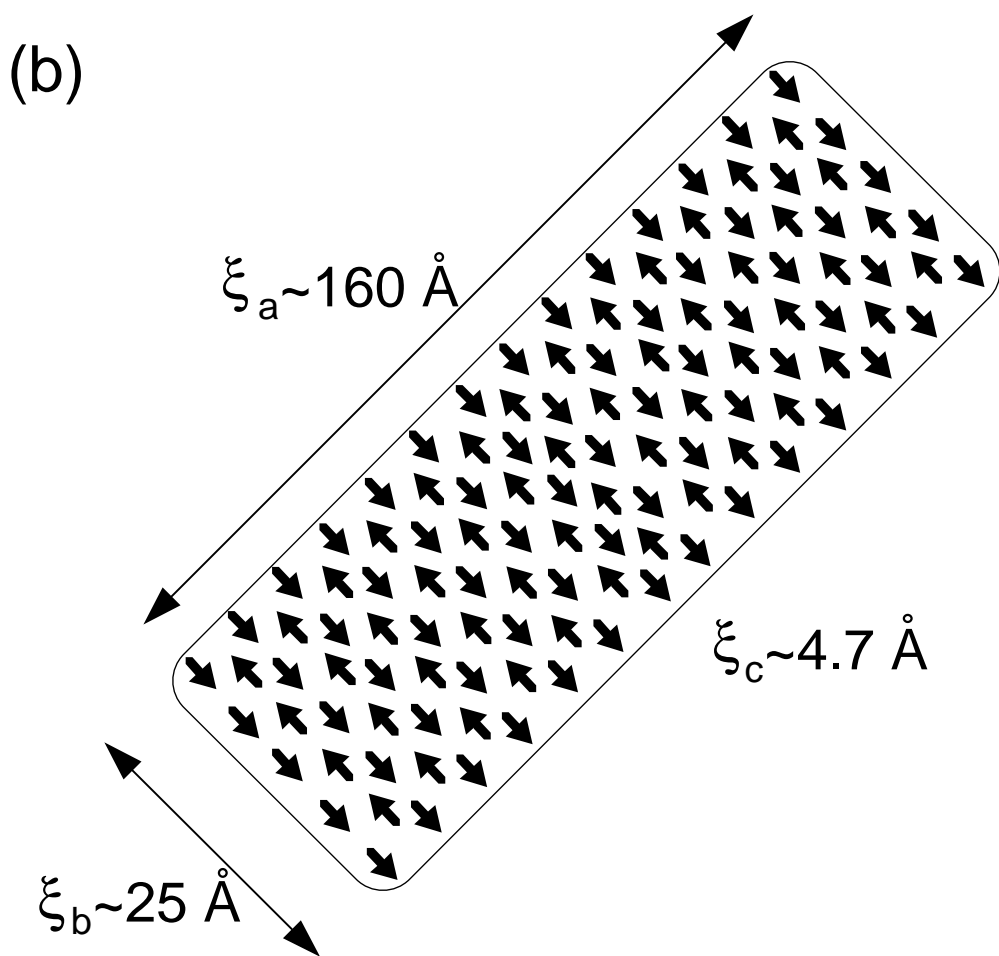
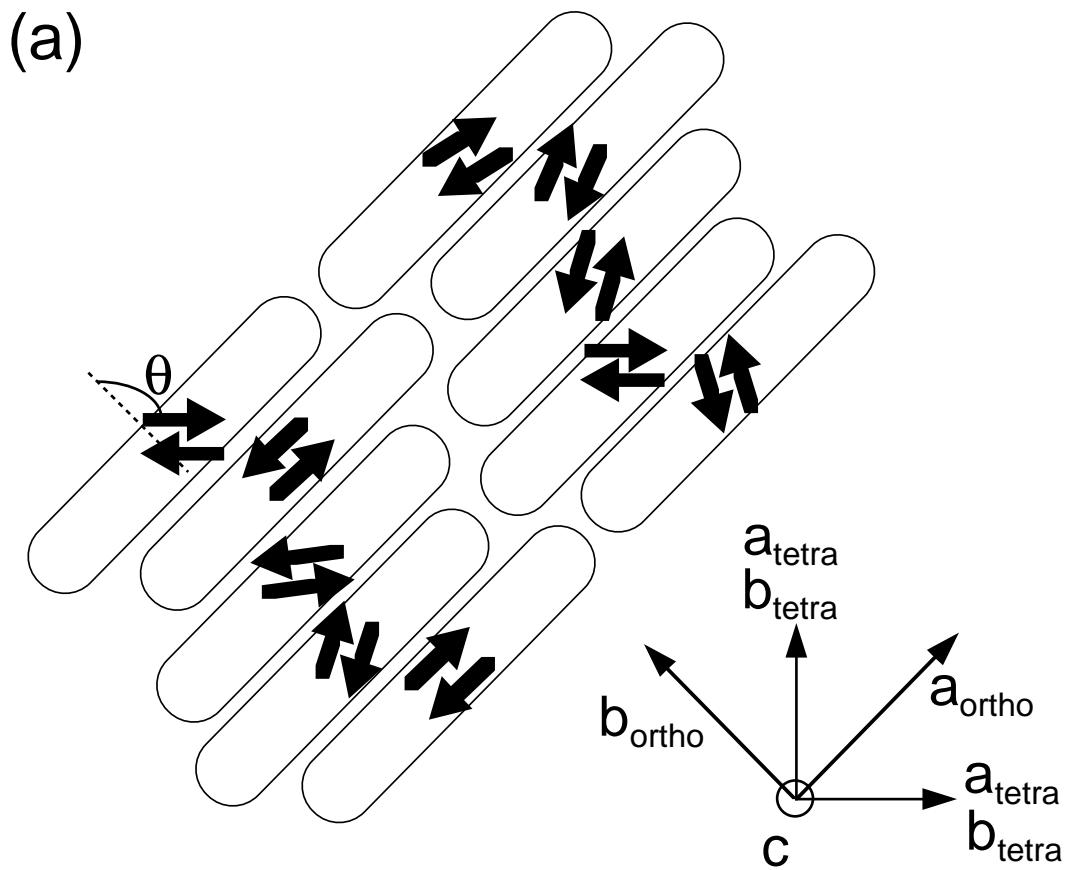


Fig. 6 Matsuda *et al.*

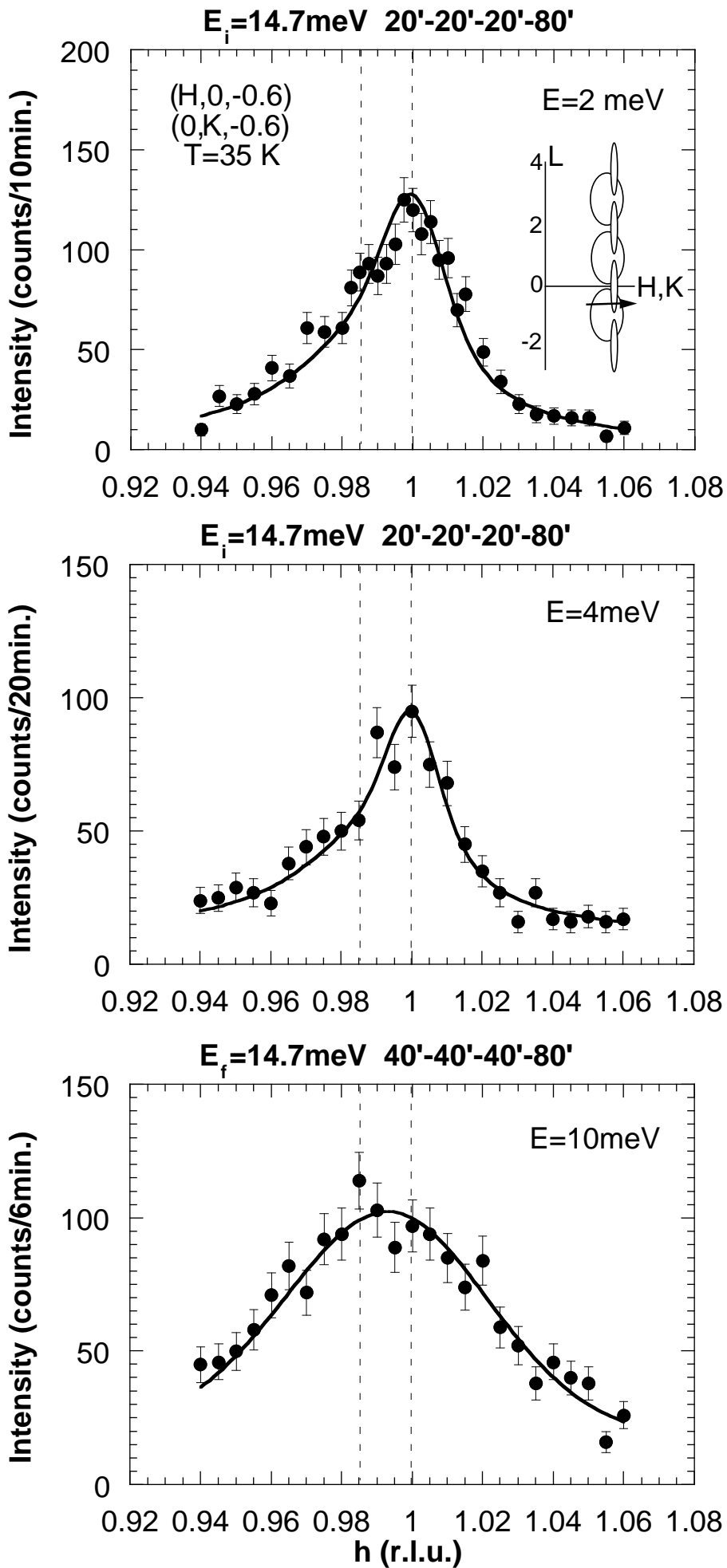


Fig. 7 Matsuda *et al.*

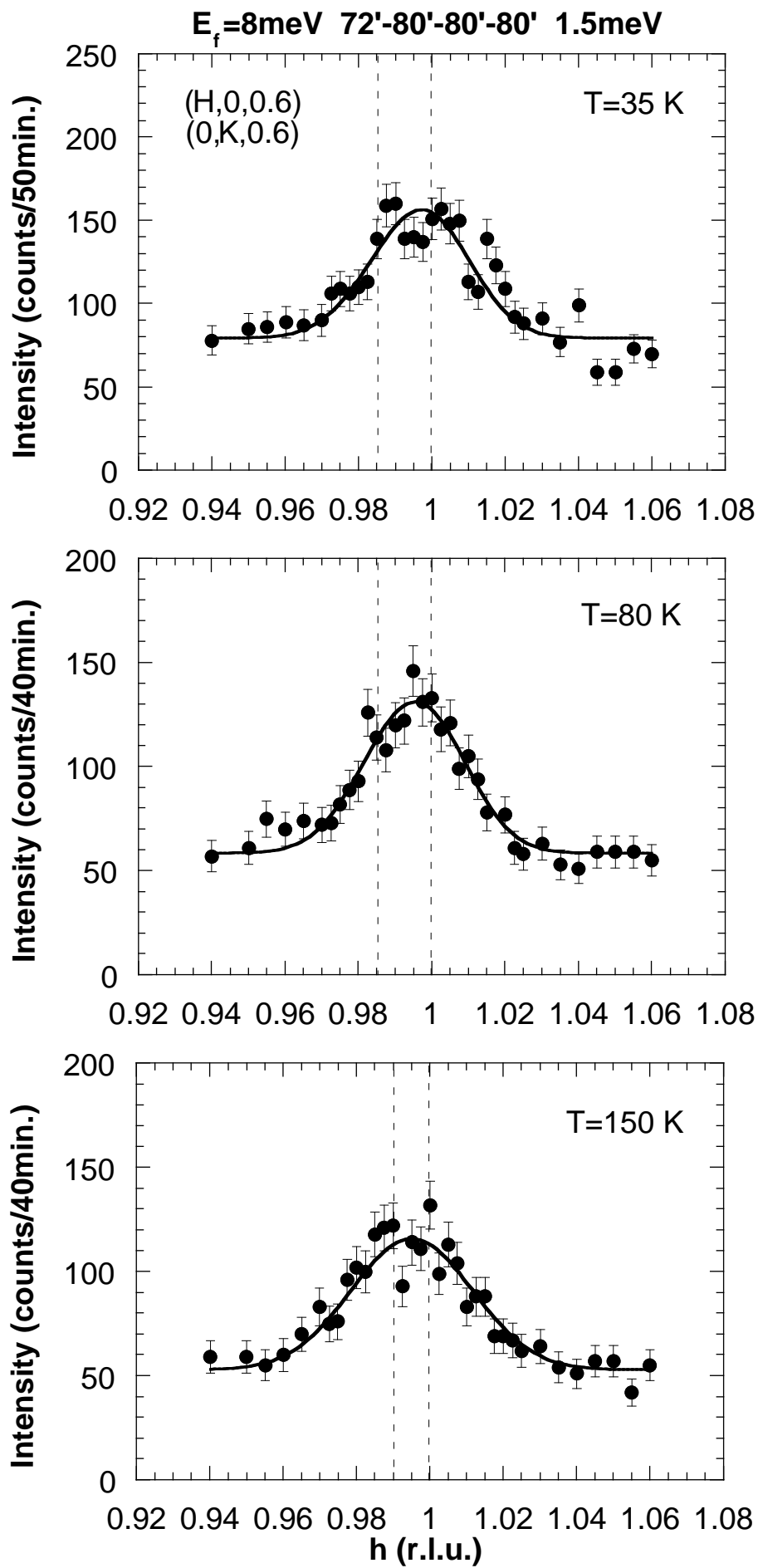


Fig. 8 Matsuda *et al.*